



A novel combination of oxidative degradation for benzotriazole removal using TiO_2 loaded on $\text{Fe}^{\text{II}}\text{Fe}_2^{\text{III}}\text{O}_4@\text{C}$ as an efficient activator of peroxyomonosulfate

Sahand Jorfi ^{a,b}, Babak Kakavandi ^{c,d,*}, Hojjatallah Ramezani Motlagh ^{a,b}, Mehdi Ahmadi ^{a,b}, Nemat Jaafarzadeh ^{a,b}

^a Environmental Technologies Research Center, Ahvaz Jundishapur University of Medical Sciences, Ahvaz, Iran

^b Department of Environmental Health Engineering, School of Health, Ahvaz Jundishapur University of Medical Sciences, Ahvaz, Iran

^c Research Center for Health Safety and Environment, Alborz University of Medical Sciences, Karaj, Iran

^d Department of Environmental Health Engineering, Alborz University of Medical Sciences, Karaj, Iran

ARTICLE INFO

Article history:

Received 19 March 2017

Received in revised form 10 May 2017

Accepted 10 July 2017

Available online 19 July 2017

Keywords:

Peroxyomonosulfate

Heterogeneous oxidation

Degradation

Benzotriazole

Wastewater treatment

ABSTRACT

A heterogeneous photocatalyst, TiO_2 -functionalized magnetic activated carbon (T@MPAC), was fabricated as a novel peroxyomonosulfate (PMS) activator for improving the oxidative degradation of benzotriazole (BTA) in aqueous media. For characterization of the features of the synthesized catalyst, XRD, FESEM, EDS, BET, TEM, PL and UV-vis DRS techniques were applied. Influence of operating parameters namely solution pH, reaction time and catalyst dosages, PMS and BTA was studied in a batch environment. A plausible oxidation mechanism and reaction pathway for BTA degradation was proposed. Potential catalytic, recyclability, durability and quenching studies were performed. The catalytic activity of T@MPAC in the activation of different oxidants also evaluated. Under optimized conditions, the degradation and mineralization rates of BTA were found to be 71.6 and 38.7%, respectively, after the fifth cycles. The catalytic activity of T@MPAC on BTA degradation was improved with the suitability in order of PMS > persulfate > ozone > H_2O_2 . The trapping experiments confirmed the participation of $\cdot\text{OH}$, $\text{SO}_4^{\cdot-}$, $\text{O}_2^{\cdot-}$ radicals as reactive species in the system. Among the reactive species (i.e. $\cdot\text{OH}$, $\text{SO}_4^{\cdot-}$, $\text{O}_2^{\cdot-}$ and holes) included in T@MPAC/PMS/UV system, $\text{SO}_4^{\cdot-}$ radicals had dominant role in controlling the oxidation reaction. Decreasing the degradation rate in the presence of scavenger agents was as IPA > BQ > *t*-BuOH > KI. The catalytic performance dropped in the presence of chloride ions, while it was less affected by phosphate, nitrate and sulfate anions. The catalyst showed a good recyclability and stability after five consecutive uses. To conclude, coupling of T@MPAC/UV and PMS can be successfully applied as a novel and effective technique to degrade organic substances in wastewater, due to easy recoverable, high catalytic activity and the cogeneration of different reactive species.

© 2017 Elsevier B.V. All rights reserved.

1. Introduction

The emerging pollutants have attracted intensive attention during the past few decades owing to their discharging into the water resource bodies. The discharge of these pollutants is potentially able to cause serious environmental pollution and human health concerns, due to their non-biodegradability and toxic nature for microorganisms and human. Benzotriazole (BTA), as an emerging pollutant, is mainly consumed in various industries, including

cutting fluids, antifreeze, hydraulic brake fluids pharmaceuticals, detergent, plastic and dye manufacturing. It is also widely used as a flame retardant in aircraft de-icers and anticorrosive additive [1–3]. The toxic and carcinogenic properties of BTA can affect organisms and human health as reported in the literature. Since BTA possess a high solubility in water (28 g/L), the monitoring and purification of water resources is a critical necessity. During previous years, several studies have been conducted on monitoring BTA in water resources and there found large amounts it in aqueous media [4,5].

In general, the conventional wastewater treatment techniques have been less effective to remove organic compounds, due to their high toxicity and chemical stability. Hence, advanced oxidation processes (AOPs) had been superior to the other methods, because of the non-selectivity and high redox potential of the hydroxyl

* Corresponding author at: Department of Environmental Health Engineering, Alborz University of Medical Sciences, Karaj, Iran. Tel.: +98 9181304929.

E-mail address: kakavandibvch@gmail.com (B. Kakavandi).

radical ($\cdot\text{OH}$) on degradation of persistent organics [6,7]. Among AOPs, photocatalyst process has proven to be the efficient technique for the treatment of organic pollutants in water because of its cost-effectiveness, high performance and lower consumption of materials and reagents. Recently, many authors have focused their attentions on titanium dioxide (TiO_2), as a semiconductor typical photocatalyst, due to its favorable performances including chemical stability, strong oxidizing power, ease of availability, robustness against photo-corrosion, economical features and toxicity [8,9]. A good efficiency of TiO_2 in organic removal can be derived from two mechanisms: adsorption onto the TiO_2 surfaces and photocatalytic oxidation, which adsorption mostly takes place much faster than photocatalytic oxidation [10].

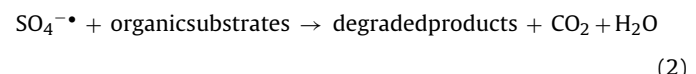
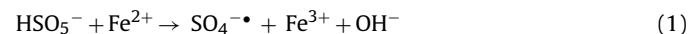
However, two problems have totally restricted the practical applications of TiO_2 : the first problem is the difficulty in disturbing single TiO_2 particles; and the second is the separation and recovery of TiO_2 nanoparticles from the reaction solution which is often a difficult and energy-consuming process. Recently, lots of research have been performed to promote the photocatalytic activity of TiO_2 particles by means of their immobilization on porous supporting materials. In this regard, large number of supports such as zeolite, clay, activated carbon, silica and graphene have been employed by researchers [8,10]. Lee et al. [11] demonstrated that in the carbon/ TiO_2 photocatalysts, the carbon materials are employed as efficient photogenerated electron acceptors, thus noticeably suppressing charge recombination and improving the rates of photocatalysis, as compared with neat TiO_2 nanoparticles.

Among these carbon-based materials, commercial powdered activated carbon (PAC) have been extensively applied as catalytic supporters in aqueous solution for contaminants removal, due, primarily, to their unique properties such as high surface area and porosity, chemical and thermal stability, high adsorption capacity, easy availability and easy recovery of expensive metal phases [12–14]. It has widely been reported that the photocatalytic degradation of organic contaminants in solution by a suspended mixture of TiO_2 and activated carbon was enhanced, due to the synergistic effect and a common contact interface between TiO_2 and activated carbon [8]. Based on these findings, many efforts have been devoted to the application of the TiO_2 -loaded activated carbon and studied the photocatalytic activity, which confirmed that the photocatalytic activity had significant improvement than the pristine TiO_2 [15–17].

However, the efficient separation and recovery of this composite from the reaction solutions have been reported as a challenge, restricting its extensive practical applications. An easy approach to tackle the separation challenge is the magnetization of photocatalysts by means of magnetic nanoparticles (e.g. magnetite, maghemite), which could be separated and recycled conveniently by applying an external magnetic field [18,19]. Herein, magnetite nanoparticles have considerable ability to be applied as recoverable photocatalysts because of their high capacity to be separated from solution through a magnet which is an effective alternative for filtration that not only enhances their catalytic potential, but also improve their recoverability.

On the other hand, magnetite nanoparticles, Fe_3O_4 , have high ability in the activation of oxidants such as hydrogen peroxide (H_2O_2), persulfate ($\text{PS}, \text{S}_2\text{O}_8^{2-}$) and peroxymonosulfate (PMS, HSO_5^-) to produce reactive species (i.e. radicals of sulfate ($\text{SO}_4^{\cdot-}$) and hydroxyl ($\cdot\text{OH}$)) for degradation of organic pollutants through the Fenton reactions [7,20,21]. In this regard, Fe_3O_4 MNPs noticeably improved the formation rate of $\text{SO}_4^{\cdot-}$, because of the existence of octahedral sites that contain Fe^{2+} ions according to Eq. (1). The produced $\text{SO}_4^{\cdot-}$ is then robust strong species reacting unselectively with organic substances leading to the mineralization of the mentioned materials into the inorganic ions, CO_2 and H_2O (Eq. (2)). Hence, a composite photocatalyst combining high surface area and magnetic separability with Fenton oxidation potential was very

attractive. In addition, it was widely reported that TiO_2 coupled with Fe_3O_4 not only represents a good magnetic response, but also displayed a high photocatalytic efficiency, which confirms the synergistic effect between TiO_2 and Fe_3O_4 in catalytic degradation processes [22,23]. Moreover, several authors observed that Fe doping on TiO_2 enhances the UV and visible light performance [24,25].



For these reasons, the current study was focused on the preparation and characterization of TiO_2 supported on magnetic activated carbon (T@MPAC) and its application as a magnetically recoverable photocatalyst in the activation of PMS on degradation of BTA. Thus, we were engaged in the coupling of adsorption and degradation (i.e., UV-Fenton and photocatalyst) processes using T@MPAC, PMS and UV to enhance the degradation rate by ways of (i) the cogeneration of active species (i.e. $\cdot\text{OH}, \text{SO}_4^{\cdot-}, \text{O}_2^{\cdot-}$ radicals) (ii) electron trapping thus limiting the rate of electron-hole recombination. To the best of our knowledge, no study so far has investigated the degradation of organic compounds by integrate of T@MAC and PMS oxidant. The influence of various input variables on the degradation efficiency was studied through response surface methodology (RSM). The photocatalytic activity, stability and recycle ability of as-synthesized catalyst was performed comprehensively. The mineralization degree of BTA under T@MPAC/PMS/UV system was studied. Moreover, a reasonable mechanism of activation and degradation was proposed.

2. Materials and methods

2.1. Chemicals

All the applied materials were of analytical grade, prepared from Merck Company (Darmstadt, Germany), and used without further purification. Deionized water (DI-water) was applied in all the experiments.

2.2. TiO_2 preparation

For preparation of TiO_2 nanoparticles, a modified sol-gel preparation method was employed. Firstly, 0.1 mol of titanium tetrakisopropoxide (TTIP) was added and dissolved in 100 mL of ethanol and stirred for 10 min to form a white sol. Subsequently, concentrated HNO_3 was added in a drop-wise state into the abovementioned solution under vigorous stirring until the white precipitate disappeared and a transparent sol was formed. The pH of sample was adjusted to 4.0. After stirring for 6 h at room temperature, a transparent yellow sol was obtained followed dried in an oven at 70 °C for 10 h and then ground in a mortar to obtain a homogeneous material. Finally, the obtained solid calcined at 450 °C in a nitrogen flow in a horizontal split tube furnace (Nabertherm GmbH, R120/500/12) for 2 h.

2.3. T@MPAC preparation

MPAC composite was synthesized using the in-situ chemical co-precipitation method under N_2 atmosphere, according to the procedure given in our previous work [12]. T@MPAC was prepared by mixing anatase-phase TiO_2 and MPAC composite in DI-water, based on dip-coating procedure. Firstly, a desired quantity of TiO_2 nanoparticles was poured in 200 mL DI-water which was followed

by stirring on a magnetic stirrer for 30 min at 25 ± 1 °C. Afterwards, 2 g of MPAC composite was added into the above mixture. The suspension was then stirred for an additional 30 min. In the following, an ultrasonic bath with high-intensity ultrasound at a frequency of 20 kHz and the electrical energy input at 100W/cm^2 was applied in order to treat the mixture for around 30 min. Here, the sonication process was conducted from the top of the glass reactor using a Sonics & Materials, Inc., VC 750 ultrasonic generator (13 mm diameter high-intensity probe, amplitude 50%). After performing the sonication treatment, to obtain a homogeneous suspension, the sample was vigorously mixed using a mechanical mixer at 500 rpm for 60 min at room temperature. The obtained solid was collected from the suspension by a magnet and rinsed sequentially with DI-water/ethanol for removal of any free TiO_2 particles that were not attached to the MPAC. It was then dried and finally annealed at 450 °C for 2 h under a nitrogen atmosphere in a muffle furnace to obtain final T@MPAC composite photocatalyst. The mass ratio of MPAC and TiO_2 was controlled at 1:2.

2.4. Characterization of T@MPAC

As-synthesized T@MPAC composite photocatalyst was characterized for their structural, morphology, textural, crystallography and physicochemical. Powder X-ray diffraction (XRD) analysis of the synthesized composite prepared at 25 °C on an X-ray diffractometer (Quantachrome, NOVA 2000) using a graphite monochromatic $\text{Cu K}\alpha$ radiation ($\lambda = 1.54\text{\AA}$) at 40 kV, 30 mA over the 2θ scanning range of 10–80°. A field emission scanning electron microscopy (FESEM, Mira 3-XMU) equipped with an energy dispersive X-ray spectrometer (EDS) was employed to characterization of the size, morphological and structural features of the samples. Transmission electron microscopy (TEM) images were prepared on PHILIPS, EM with high-resolution at 100 kV for characterization of the size and morphology of the prepared nanoparticles. The Brunauer–Emmett–Teller (BET) surface area, adsorption isotherms, pore volumes, and pore size distribution of the samples were determined via a Quantachrome, NOVA 2000 physical adsorption apparatus at 77 K. The magnetic features of catalysts were evaluated using vibrating sample magnetometer (VSM, 7400, Lakeshare, USA) at room temperature. Optical properties of the prepared samples were analyzed using a UV–vis diffuse reflectance spectroscopy (DRS) over a range of 190–800 nm in the absorption mode on a U-3900 Spectrophotometer (Hitachi Ltd., Japan) with BaSO_4 as a reflectance standard. Also, photoluminescence (PL) spectra of the samples were measured at room temperature by a fluorescence spectrophotometer (Perkin Elmer, LS 55, USA) with an excitation wavelength of 300 nm.

2.5. Dark adsorption studies

In order to obtain the adsorption-desorption equilibrium behavior among the catalyst and BTA, a series of batch tests were conducted under ambient temperature before UV irradiation and adding PMS as follows: a desired amount of T@MPAC catalyst was added into 100 mL of 50 mg/L BTA solution. The samples were wrapped with aluminum foil to minimize light exposure which was followed by agitation using a shaker at a constant rate of 200 rpm within 180 min. At selected time intervals, after magnetically separation of catalyst, the residual BTA concentration was measured. In the following, the adsorption kinetics and isotherms studies were performed to adsorption process modelling.

2.6. Catalytic activity experiments

Lab-scale catalytic reactions (i.e. photocatalyst and UV-Fenton) were performed in a batch reactor and a 500-mL cylindrical quartz

vessel containing 200 mL of sample. After the adsorption saturation, by addition of a known amount of PMS into them and then immediately placed vertically near a light source (UV-C lamp, 6W PHILIPS) at a distance of 1 cm to start the UV-assisted oxidation reactions. The reaction mixture was stirred well at 200 rpm by a mechanical stirrer for 120 min. After a defined time interval, the catalyst was separated using a magnet and the residual BTA concentration was determined using a high-performance liquid chromatography (HPLC). To prevent further side reactions, 2 mL of 0.2 M sodium thiosulfate ($\text{Na}_2\text{S}_2\text{O}_3$) was added immediately to the supernatant before the analysis. The BTA removal under different systems was also carried out as control experiments to comparison between systems.

2.7. Analysis and measurement methods

BTA concentrations were measured using an HPLC (model KNAUER, Germany) equipped with ultimate variable wavelength UV detector (2500), according to the procedure employed in our previous work [26]. The by-products formed during the BTA degradation were also identified using HPLC by comparison with the retention time of the standard compounds. The analysis was carried out in duplicate to confirm reproducibility. Mineralization efficiency was monitored by measuring the total organic carbon (TOC) with a Shimadzu VCHS/CSN, Japan. Furthermore, Fe concentration leached in the solution was determined using an atomic absorption spectrophotometer (AAS, Analytikjena vario 6, Germany), according to ASTM D1068-90 to evaluation of catalyst stability [27].

2.8. Experimental design and procedure

In the present study, the central composite design (CCD) under RSM was used to design the experiments for finding the mutual effects of the influencing experimental variables and for optimizing the removal of BTA by T@MPAC/PMS/UV system. The influence of operating parameters namely pH of solution, catalyst dosage, reaction time, initial BTA concentration and PMS concentration on the process performance were investigated in a batch system. The effect of parameters was evaluated at five various levels coded, according to Table 1. Based on the CCD matrix, 48 experimental runs were conducted for five independent parameters (Table S-1).

3. Results and discussion

3.1. Analysis of T@MPAC characterization

In our previous work, we observed that the external surface of PAC is more porous than MPAC composite, due to the filling of some pores with Fe_3O_4 nanoparticles during the magnetization process [12]. Fig. 1 shows the FESEM micrograph coupled with EDS for MPAC, TiO_2 and T@MPAC composite. Fig. 1(a) reveals that the MPAC is still porous and its external surface is rough and has some reactive sites, demonstrating the good capability of the synthesized composite for adsorbing contaminants. Also, uniform distribution of Fe_3O_4 MNPs is observed noticeably on MPAC surface, providing a high catalytic activity for composite in oxidation processes. Results of EDS analysis (Fig. 1(a)) elucidated that both dopant elements (i.e., Fe and O) were presented in the structure of as-synthesized composite. A high peak assigned to carbon is also observed in the EDS spectrum, which confirms that the carbon contents still exist on the surface of the composite after magnetization process. Moreover, no characteristic peaks of impurities are observed in the EDS spectrum, implying that the as-synthesized composite possess a high purity. The FESEM image of TiO_2 (Fig. 1(b)) depicts that the particle distribution of synthesized TiO_2 was approximately uniform with an average diameter of $<20\text{ nm}$. High purity of synthesized TiO_2 was

Table 1

Independent variables and their levels in the experimental design.

Independent factors	Symbols	Ranges and levels					Unit
		-2	-1	0	+1	+2	
pH	A	2	4	6	8	10	
Catalyst loading	B	0.1	0.2	0.3	0.4	0.5	g/L
Initial BTA concentration	C	20	40	60	80	100	mg/L
PMS dosage	D	1	2	3	4	5	mM
Reaction time	E	10	30	50	70	90	min

verified using EDS analysis (Fig. 1(b)), where characteristic peaks of impurities are not observed in the EDS spectrum. For T@MPAC composite, the FESEM analysis (Fig. 1(c)) exhibits that both Fe₃O₄ and TiO₂ nanoparticles were deposited homogeneously onto the external surface as well as within of the pores of the PAC. It can be seen the presence of some reactive sites in the composite structure, illustrating a relatively good porosity for sorption of contaminants. The presence of both Fe and Ti elements also was confirmed in EDS spectrum, as shown in Fig. 1(d). Besides, the noticeable amount of carbon element indicates that the carbon contents still exist on the surface of the composite after impregnation process. Generally, these results proved the successfully coating of Fe₃O₄ and TiO₂ onto the PAC surface.

TEM micrographs (Fig. 2) show that the both Fe₃O₄ and TiO₂ particles were almost well dispersed within PAC surface with the average side length of 30 and 50 nm, respectively. It also reveals a spherical structure for Fe₃O₄ nanoparticles which is consistent with the results of XRD analysis.

The XRD patterns of MPAC, TiO₂ and T@MPAC are shown in Fig. 3(a). All diffraction peaks correspond to carbon and Fe₃O₄ particles were observed in the XRD spectra of MPAC without remarkable changes in the basic of their diffraction peaks. In this pattern, it can be seen clearly a broad peak at 2θ value of 25° for carbon along with six sharp peaks at 2θ values of 30.07°, 35.44°, 43.15°, 54.6°, 56.99°, and 62.6° for Fe₃O₄ particles, suggesting successful synthesis of Fe₃O₄ crystals with high purity on the carbon surfaces. The XRD spectrum of the synthesized TiO₂ matches well with the pattern of standard titanium oxide nanoparticles based on the JCPDS card no. 21-1272, implying TiO₂ was quite similar to that of pure titanium oxide anatase phase. Hence, for the prepared TiO₂, anatase was assumed as a prominent phase, which is beneficial, because of its higher photocatalytic activity. The XRD pattern of TiO₂ confirms that all the characteristic peaks correspond to the TiO₂ anatase phase and no rutile phase was detected. As shown in Fig. 3(a), the XRD spectra of T@MPAC includes all of the above-mentioned peaks without detectable damage in the basic of carbon, TiO₂ and Fe₃O₄ framework and it was match together very well. In the X-ray spectrum of T@MPAC, it is noteworthy that the peak belonged to carbon at 2θ=25° was narrower and sharper than that of the MPAC pattern. This can be attributed to the characteristic reflection of TiO₂ at 2θ values of 25° according to the X-ray diffractogram of TiO₂. The average diameter of Fe₃O₄ and TiO₂ was determined using Debye–Scherrer equation as 32 and 54 nm, respectively, which were in a good agreement with those measured by TEM analysis.

The results obtained from analysis of physico-chemical characteristics of different samples by BET (Table 2) implied that the specific surface area of PAC showed a decreasing trend from 744.8 to 572.6 and 269.5 m²/g after the loading of Fe₃O₄ and TiO₂ nanoparticles, respectively. This reduction can be referred to the blockage of PAC pores with both Fe₃O₄ and TiO₂ nanoparticles coverage. BJH pore size distribution demonstrates that the average pore diameters of all samples were in the range of 2–50 nm, indicating their mesoporous structures, based on the IUPAC classification. The N₂ adsorption-desorption isotherm of the MPAC and T@MPAC also presents a type IV isotherm (Fig. 3(b)) as categorized

by the IUPAC, which confirms mesoporous structures of prepared catalyst.

VSM magnetization curve of the as-synthesized catalysts at 25 °C in the magnetic field of ±10 kOe are presented in Fig. 3(c). Considering the obtained results, highest magnetic saturation 74.6 emu/g was assigned to Fe₃O₄ nanoparticles, whereas the values of 35 and 25.3 emu/g were obtained for MPAC and T@MPAC catalysts, respectively. These differences can be mostly attributed to the contribution of the presence of non-magnetic materials (i.e., PAC and TiO₂) in the catalyst texture. Although the magnetic saturation value of T@MPAC catalyst was lower magnetic bare Fe₃O₄ nanoparticles, the catalyst showed an excellent magnetic response in the presence of an external magnetic field (inset Fig. 3(c)), indicating that T@MPAC can be quickly collected from aqueous media and utilized as a recyclable magnetic catalyst for environmental clean-up applications without generating secondary pollution.

UV-vis DRS spectra can provide information about the ability of samples to generate electron–hole pairs under the light irradiation. The DRS spectra patterns of TiO₂, MPAC and T@MPAC in Fig. 4(a), display a narrow light-response range for pure TiO₂ nanoparticles. It can be seen a strong absorbance just below 400 nm for pure TiO₂ nanoparticles, which can be due to its band gap excitation. As observed, both MPAC and T@MAPC showed adsorption area wider compared with spectrum of TiO₂, indicating that T@MPAC can be activated by visible-light. It is clear from Fig. 4(a) that the absorption peak assigned to T@MPAC shifted towards longer wavelength and was total over all range of the measured UV-vis region. This can be derived from the composition overlapping absorption spectrum of TiO₂ and carbon. A good absorption intensity of T@MPAC in both UV and visible light regions suggests that introduction of MPAC was favorable for the absorption light of TiO₂. These results also reveal that the incorporation of MPAC and TiO₂ enhances the photocatalytic performance them over visible-light. The results of PL spectrum (Fig. 4(b)) exhibit that PL spectra patterns of samples were different in broad PL emission peak and PL intensity. A broad PL emission peak at near 564.4 nm was observed for TiO₂, while it was 626.2 and 659.5 nm respectively for MPAC and T@MPAC samples. It also found that PL intensity of TiO₂ was significantly higher than the other samples, implying both carbon and Fe₃O₄ have important role in suppress the recombination of excited holes and electrons. Furthermore, a lower PL intensity for the T@MAC in comparison with TiO₂ and MPAC depicts that the combination of TiO₂ and MPAC could improve the efficiency of the electron–hole separation which consequently led to enhancement of the photocatalytic activity for the as-synthesized catalyst.

3.2. Dark adsorption capability of T@MPAC

Adsorption has been considered as an important step of heterogeneous photocatalysis. Due to high adsorption capability of PAC, it was necessary to employ dark adsorption experiment to T@MPAC. In this work, the adsorption experiments were carried out before the photocatalytic tests. Fig. 5(a) shows the kinetics of BTA adsorption onto PAC, MPAC and T@MPAC during 180-min time under the same conditions. The adsorption rate was very quick dur-

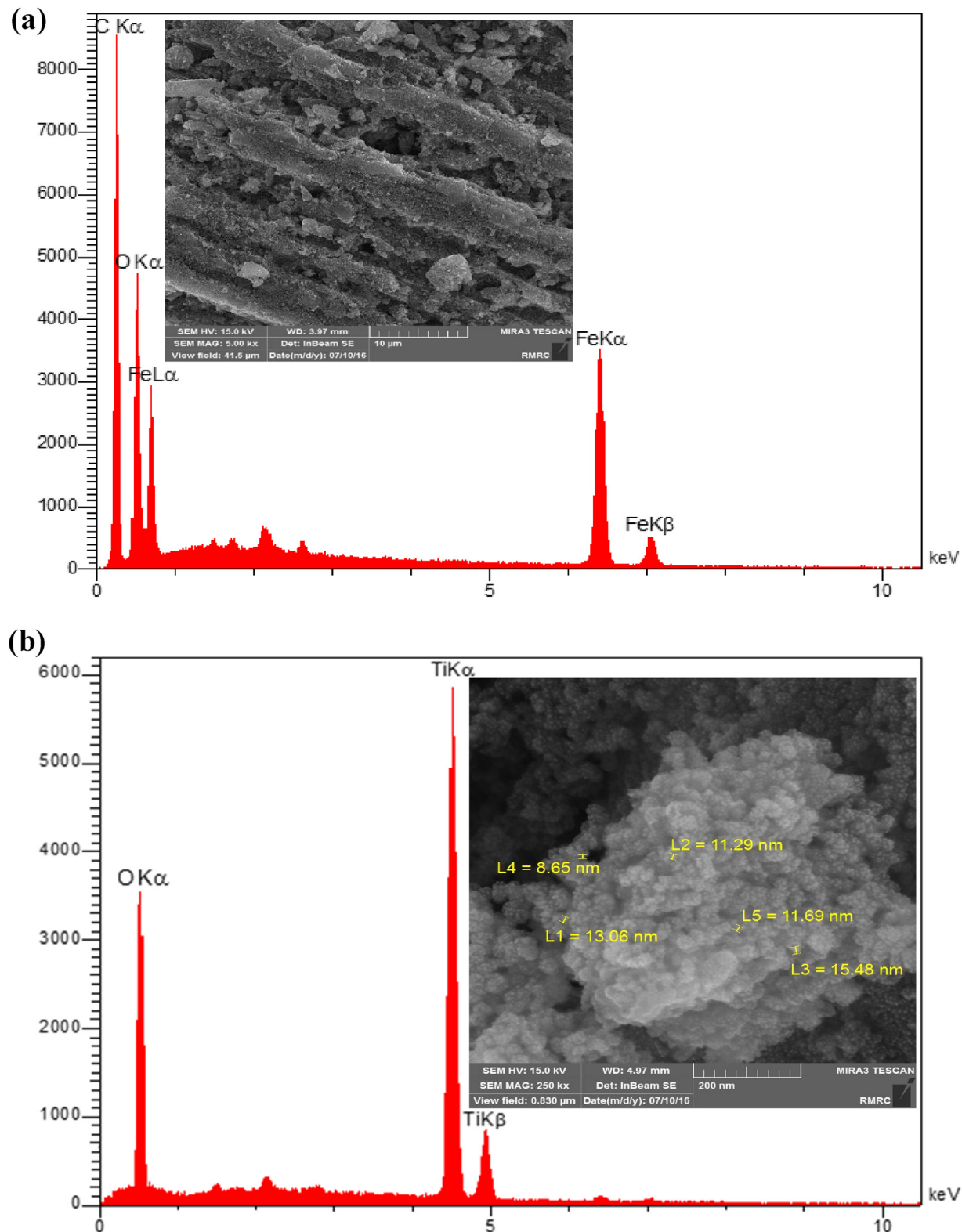


Fig. 1. FESEM and EDS analyzes of MPAC (a) and TiO₂ (b), FESEM image of T@MPAC (c) and EDS spectrum of T@MPAC (d).

ing the initial stage ($t < 60$ min) for all adsorbents, which suggest the occurrence of a physical adsorption process [28,29]. For further times, however, no significant changes were observed, implying that the adsorption process had already reached the equilibrium state at 60 min. The adsorption efficiency for PAC was higher significantly than that obtained for other adsorbents, which could be

explained by the large porosity and high surface area of PAC. On the other hand, T@MPAC shows a better adsorption capability for BTA removal compared to MPAC, indicating the loading TiO₂ nanoparticles on MPAC enhance the adsorption capacity of MPAC for BTA. Furthermore, the removal efficiency 38.6% for 40 mg/L of BTA by T@MPAC suggests a good adsorption performance for the prepared

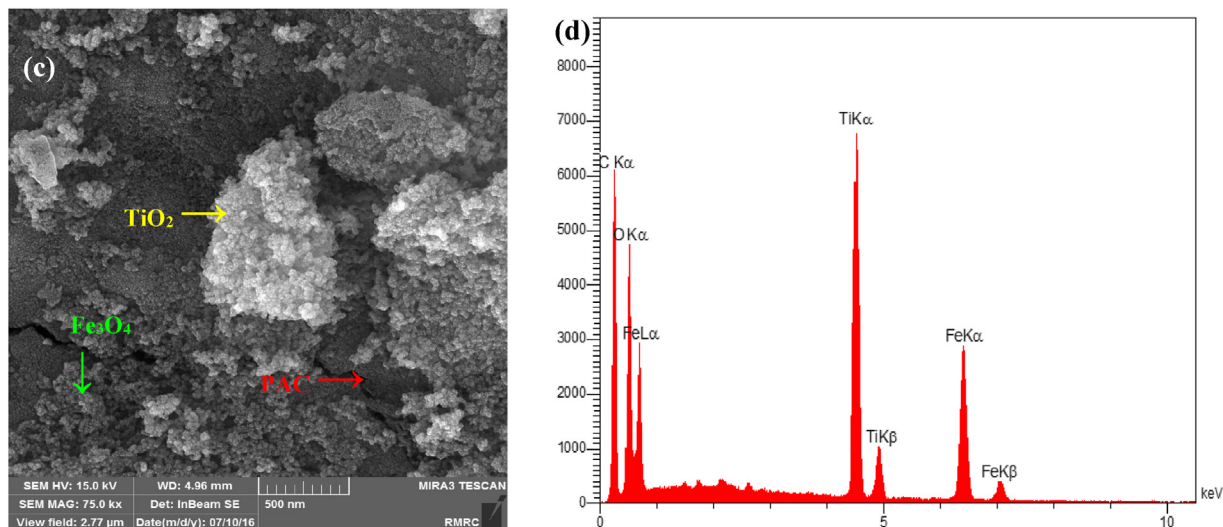
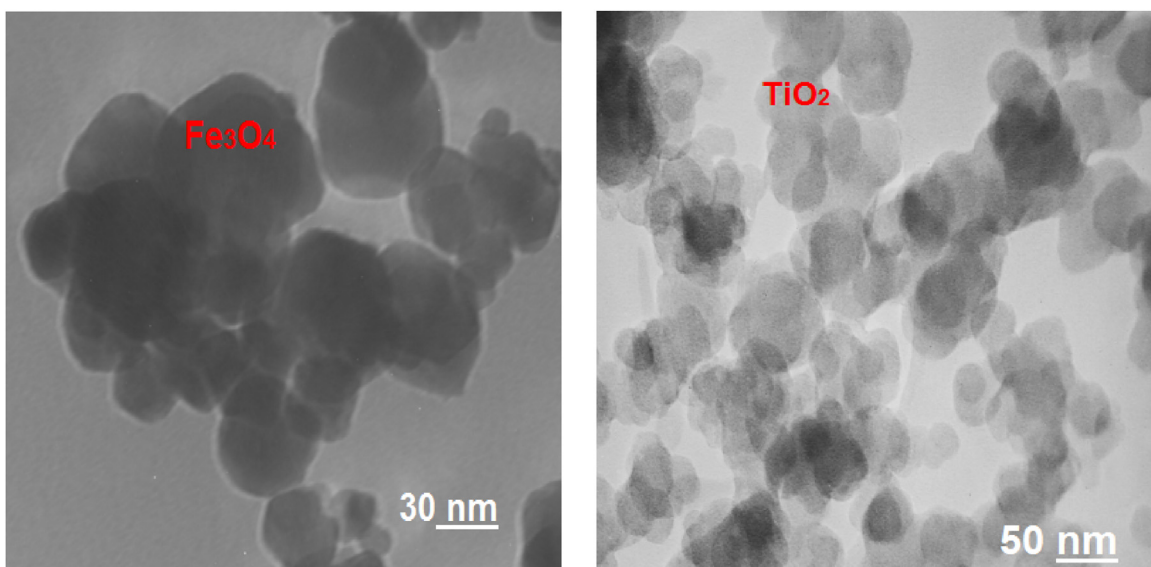


Fig. 1. (Continued)

Fig. 2. TEM images of Fe_3O_4 (a) and TiO_2 (b) nanoparticles coated on PAC.**Table 2**

Physicochemical characteristics of applied materials in this study.

Sample	$S_{\text{BET}}(\text{m}^2/\text{g})$	V_t^{a} (cm^3/g)	V_m^{b} (cm^3/g)	D_p^{c} (nm)	Pore structure	Color
Fe_3O_4	63.2	0.006	36.7	2.95	Mesopore	Black
PAC	744.8	0.462	186.52	4.33	Mesopore	Black
MPAC	572.6	0.3792	114.43	3.04	Mesopore	Black
TiO_2	41.4	0.084	21.3	2.9	Mesopore	White
T@MPAC	269.5	0.433	61.8	6.43	Mesopore	Black

^a V_t denotes the total pore volume.

^b V_m denotes the monolayer volume.

^c D_p denotes the average pore diameter.

composite on BTA adsorption. Thus, we applied 60 min of dark adsorption to all photodegradation process before UV irradiation and/or PMS addition.

Kinetic and equilibrium studies of BTA adsorption on T@MPAC was carried out to modeling the adsorption process. The results revealed that BTA adsorption on T@MPAC can be described in a good agreement with pseudo-second-order and Freundlich models. The values of kinetic and isotherm models constants of BTA adsorption process are summarized in Table S-2. The maximum

mono-layer adsorption capacity of 351.7 mg/g was obtained based on the Langmuir model, indicating the as-synthesized composite had a high adsorption capacity for the adsorption of contaminants.

3.3. Testing of catalyst activity and control experiments

The photocatalytic efficiency of the synthesized T@MPAC on BTA removal was compared with a series of control experiments, and all

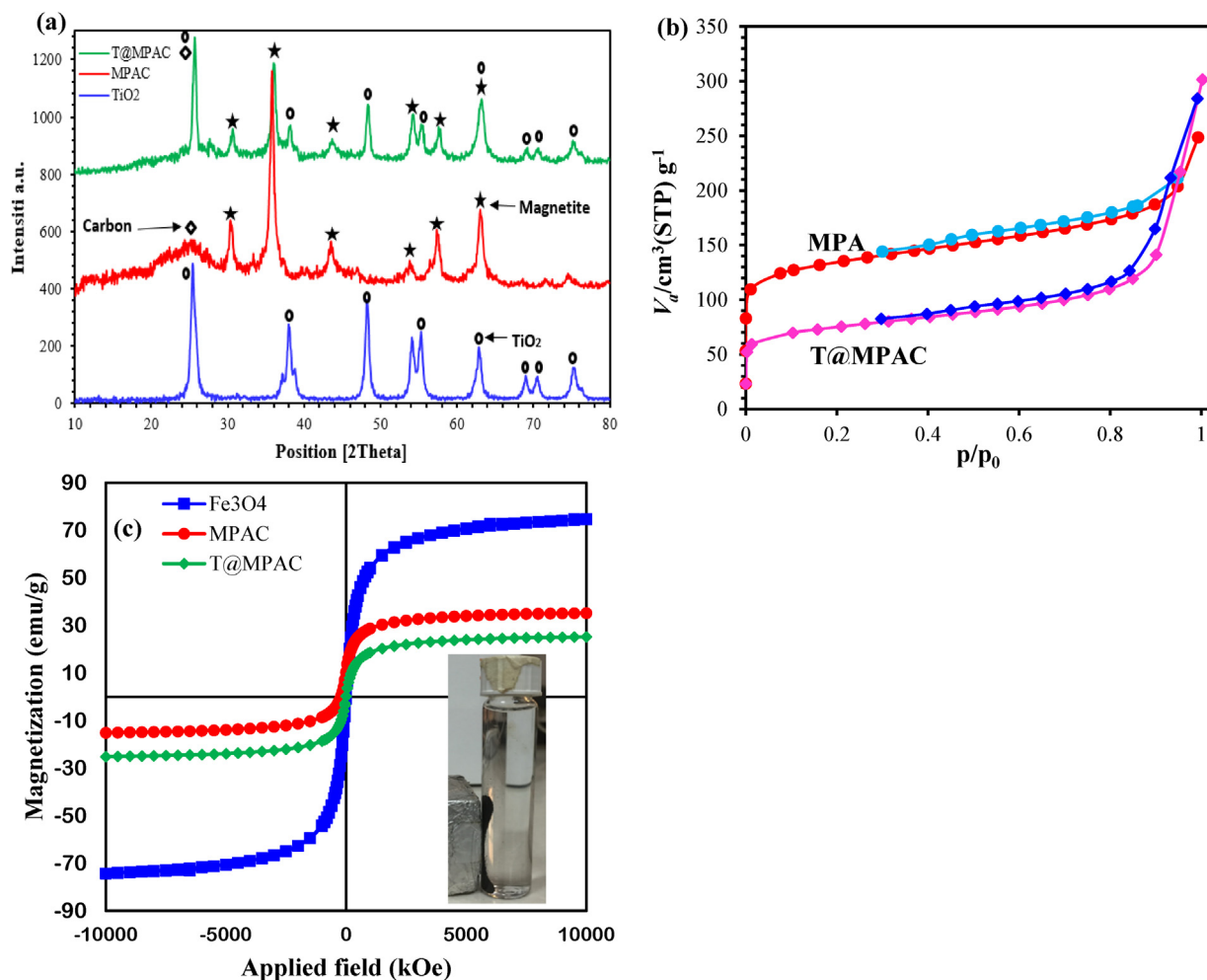


Fig. 3. (a) XRD patterns of pure TiO₂, MPAC and T@MPAC composite, (b) N₂ adsorption-desorption isotherm of the MPAC and T@MPAC and (c) hysteresis loops curves of Fe₃O₄, MPAC and T@MPAC.

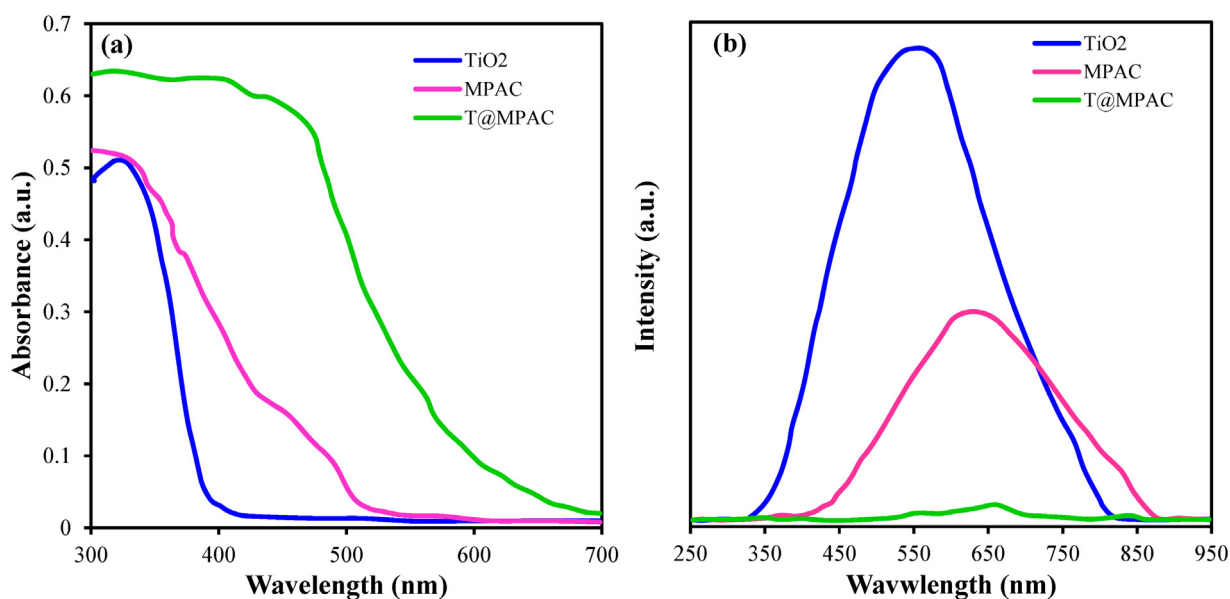


Fig. 4. UV-vis DRS spectra (a) and PL spectra (b) for the TiO₂, MPAC and T@MPAC.

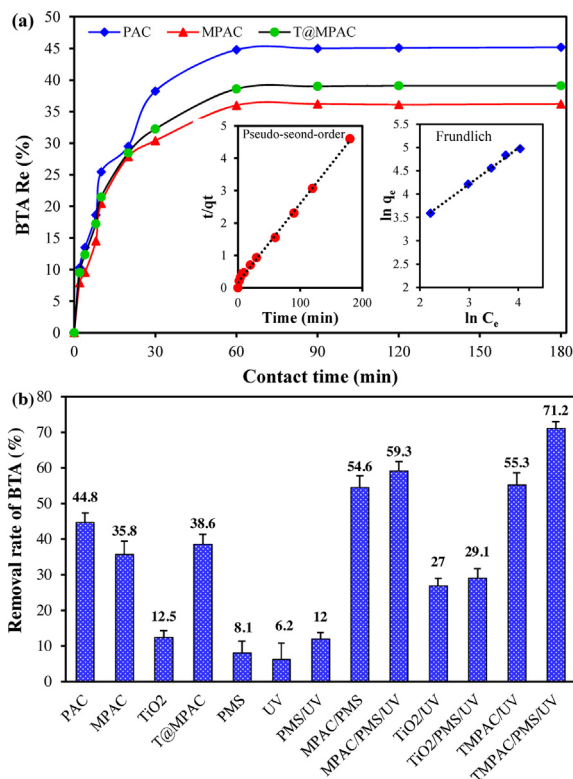


Fig. 5. (a) Adsorption of BTA on PAC, MPAC and T@MPAC within 180 min at pH 6 ± 0.2, 0.3 g/L adsorbent and 40 mg/L BTA; (a1) kinetic of BTA adsorption on T@MPAC, (a2) equilibrium isotherm of BTA adsorption on T@MPAC (20–100 mg/L BTA), (b) the removal potential of BTA by different systems (0.3 g/L catalyst (PAC, MPAC, TiO₂ and T@MPAC); 4 mM PMS, 60 mg/L BTA and 60 min reaction time).

the experiments were carried out in a 60 min time period. Fig. 5(b) represents the removal efficiency of BTA using different processes under similar experimental conditions. The adsorption processes (e.g., PAC, MPAC, TiO₂ and T@MPAC) showed higher removal rates of BTA, compared to UV and PMS both alone and together. The removal rates of 6.2, 8.1 and 12% were obtained for UV, PMS and PMS/UV systems, indicating the lower oxidation potential of these systems, and the consequently BTA cannot be degraded effectively by UV, PMS and PMS/UV systems. Referring Fig. 5(b), the Fenton processes that were included MPAC/PMS and MPAC/PMS/UV displayed the higher removal efficiencies for BTA removal, in comparison with the above-mentioned systems. The removal rates of 54.6 and 59.3% were achieved using Fenton (i.e., MPAC/PMS) and UV-Fenton (i.e., MPAC/PMS/UV) during 60 min oxidation reaction. This enhancement can be explained by the simultaneous presence of adsorption and degradation processes as well as synergistic effect of MPAC and UV irradiation on the decomposition of PMS with consequent formation of reactive species ($\text{SO}_4^{\cdot-}$) for BTA degradation [1,30,31]. These results certificated that the MPAC acted as an excellent Fenton-like catalyst and also its catalytic activity in the presence of UV improved by adding PMS to the reaction.

As can be seen, the synergistic effect between the prepared T@MPAC and simulated UV represents a removal efficiency up to 55% via photocatalysis, which was significantly greater than conventional photocatalyst system (i.e., TiO₂/UV). This reveals the critical requirement for the modification of neat TiO₂ nanoparticles for enhancing the photocatalytic removal. Moreover, since the catalysts have the similar amount of loadings (0.3 g/L), T@MPAC in comparison with bare TiO₂ reveals higher capability of removing BTA, although it naturally contained a much lower TiO₂ content, in comparison with pure photocatalyst. Our findings also illustrated that the heterogeneous photocatalysts are not only easily

recovered, but also show a high performance rather than homogeneous photocatalysts (i.e., TiO₂/UV), because both adsorption and degradation processes are simultaneously involved in the removal of pollutant. Similar observation was also reported when supported-TiO₂ materials were compared with TiO₂ alone for various pollutants degradation [8,17,32–34].

In addition, it was seen that since BTA in the solution was exposed to the combination of T@MPAC and PMS in the presence of UV light, the removal percentage of BTA significantly increased and reached 71.2% under 60 min of irradiation. However, exposure of BTA to TiO₂, PMS and UV displayed just 29% removal efficiency. This suggests that the T@MPAC not only has an excellent photocatalytic activity, but also possess a good catalytic potential in the activation of PMS. This as-synthesized catalyst, therefore, paved the way of performing further experiments on photodegradation optimization.

3.4. Operating parameters effect on catalytic performance of BTA

The combined effect of operational parameters on the performance of T@MPAC/PMS/UV system is illustrated in Fig. 6(a). According to the figure, an increase in both PMS and catalyst loading enhanced BTA removal. More than 60% of the total BTA removal was obtained when both the PMS and catalyst concentrations were at their maximum levels. Similar trends have been reported in the literature [35–37]. At higher PMS concentrations, higher amount of sulfate radicals can be generated, which resulting in more degradation of BTA. At low PMS concentration, however, an adequate number of sulfate radicals which contributes to low oxidation rate, and reducing removal efficiency cannot be formed [38,39]. An improvement in the system efficiency by enhancement the amount of catalyst can be ascribed to increasing of Fe (Fe_3O_4) quantity and photon absorption (TiO₂) on the catalyst surface; the more presence of active sites for producing free radicals, which resulting in promotion of the degradation efficiency [37]. Moreover, an increase in the catalyst loading enhanced the adsorption rates of pollutants and PMS molecules on the catalyst surface through enhancement of the quantity of reactive sites, which subsequently led to the enhancement of the decomposition of PMS and the oxidation reactions rate [40].

The simultaneous effects of the catalyst dosage and initial BTA concentration exhibit that the percentage of BTA degradation dramatically decreased with increasing BTA concentration (Fig. 6(b)). As observed, BTA removal rate decreased from 99 to 59.4% as initial BTA concentration increases from 10 to 100 mg/L, when PMS amount and pH were kept constant. Here, higher BTA concentrations could inhibit the reaction of PMS at the redox-active centers on the catalyst surface. In addition, with increasing BTA concentration, more molecules were adsorbed onto the catalyst surface and the reactions between UV light and TiO₂ were restricted; then, the generation of free radicals (e.g., HO^{\cdot} and $\text{SO}_4^{\cdot-}$ radicals) was reduced [36]. In addition, the intermediates may compete with the parent compounds for reactive radicals. On the other hand, an enhancement in degradation at lower concentrations of BTA can be explained by the presence of sufficient and/or higher than the consumption of free radicals.

The interactive effect of solution pH and PMS concentration is shown in Fig. 6(c). As observed, there was no-significant influence of solution pH on the system efficiency. At the same experimental conditions, BTA removal rates of 54.1, 48.6 and 56.2% were achieved for pH values of 2, 6 and 10, respectively. It above mentioned that the pH_{ZPC} of the catalyst was 6.5, means that the catalyst surface is positive and negative respectively at lower and higher values of pH 6.5. On the other hand, pK_a equal to 8.2 reported for BTA, which is positively charged below pH 8.2. Hence, regarding to pK_a value of BTA (8.2) and pH_{ZPC} of the catalyst (6.5), it is expected that efficient

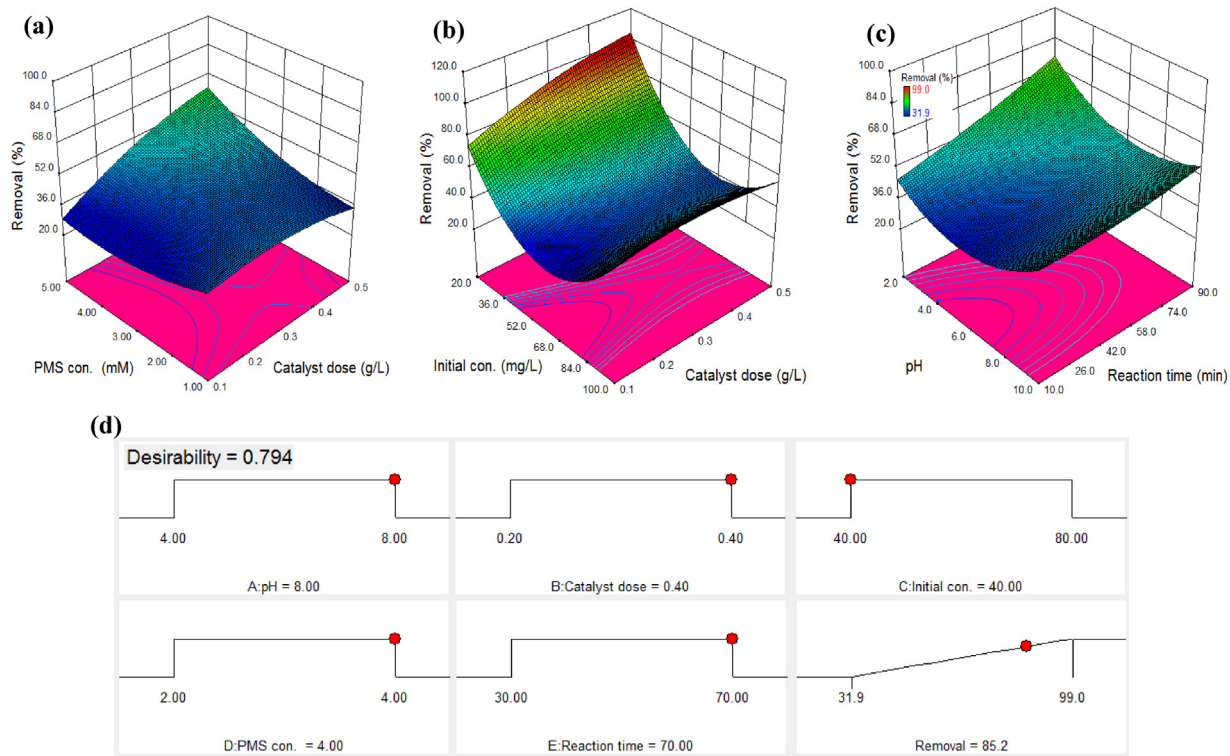


Fig. 6. (a) 3D response surfaces under CCD for BTA degradation as a function: (a1) Re% BTA vs. PMS concentration and catalyst dosage, (a2) Re% BTA vs. catalyst dosage and BTA concentration, (a3) Re% BTA vs. pH and reaction time, and (b) desirability ramp for numerical optimization of six goals solution pH, catalyst dose, BTA concentration, PMS concentration, reaction time and degradation efficiency.

removal of BTA were take place at $\text{pH}_{ZPC} < \text{pH} < \text{pK}_a^{\text{BTA}}$, where the cationic form of BTA molecules are easily adsorbed by the negative charge of T@MPAC surface. Therefore, pH 7 is suitable since it was near the neutral condition which would be able to its application for pollutants degradation without pre-adjustment of pH. Fig. 6(c) also depicts that the increasing the reaction time was favorable to promote the degradation efficiency. This issue can be attributed to the additional formation both of HO^\bullet and $\text{SO}_4^{\bullet-}$ free radicals during the T@MPAC/PMS/UV process.

3.5. Optimization of operating conditions

In order to obtain the highest possible BTA removal, the optimum values of parameters were determined using the optimization of operating conditions by numerical technique built in the Design Expert 10.0 software. In this regards, the desired goal for the BTA removal efficiency (i.e., response) defined as “maximum” whereas the studied parameters were placed “in range”. Under optimum conditions (pH 7.0, 0.4 g/L catalyst, 4 mM PMS, 40 mg/L BTA and 70 min reaction time), the maximum degradation of 85.4% was predicted by software with 0.792 desirability. Fig. 6(d) exhibits numerical optimization of six goals for the studied process. To the validation of the model predicting, a series additional experiments were performed in triplicate under above-mentioned optimum conditions. A degradation efficiency of 89.6% was obtained from experiments, which was in good agreement with the value predicted from the quadratic model, confirming the accuracy and validity of the model approach and reliability of RSM.

3.6. Catalytic potential and quenching studies

The catalytic potential of as-synthesized catalyst in T@MPAC/PMS/UV system was determined at optimum experimental conditions using Eq. (3). Where, $R_{\text{T@MPAC/PMS/UV}}$, R_{UV} , R_{TiO_2} ,

R_{PMS} and R_{ads} are BTA removal percentages by various processes. According to Fig. 7(a), it was observed a catalytic potential of 18.4% for T@MPAC on the T@MPAC/PMS/UV system. These results demonstrate that the T@MPAC catalyst has a synergistic effect on the BTA degradation in the presence of the other applied agents in the T@MPAC/PMS/UV system. It can be also stated that the catalytic role of T@MPAC is dependent of the adsorption and it can effectively enhance the removal efficiency of BTA degradation. This significant catalytic potential probably associated with the decomposition of PMS molecules and also photocatalyst reactions between TiO_2 and UV.

$$\begin{aligned} \text{Catalyticpotential}(\%) = & R_{\text{T@MPAC/PMS/UV}} \\ & - (R_{\text{UV}} + R_{\text{TiO}_2} + R_{\text{PMS}} + R_{\text{ads}}) \end{aligned} \quad (3)$$

In T@MPAC/PMS/UV system, it was expected that the presence of $\cdot\text{OH}$, $\text{SO}_4^{\bullet-}$, $\text{O}_2^{\bullet-}$ and holes as reactive species are responsible for BTA degradation. In this work, *tert*-butyl alcohol (*t*-BuOH), benzoquinone (BQ) and potassium iodide (KI) were employed as specific scavengers of $\cdot\text{OH}$, $\text{O}_2^{\bullet-}$ and holes, respectively. Also, isopropanol (IPA) was used as an effective quenching agent for both $\cdot\text{OH}$ and $\text{SO}_4^{\bullet-}$ radicals [41,42]. These scavengers can either prevent or at least decelerate the reaction process thereby filling the surface active sites of the catalyst. Besides, they can react with reactive species both generated on the catalyst surface and in the solution [43]. In Fig. 7(b), it was observed that the degradation efficiency of BTA reduced from 88.6 to 32.7, 59.5, 45.6 and 74.4%, respectively in the presence of IPA, *t*-BuOH, BQ, and KI scavengers. The obtained results of quenching experiments revealed that four reactive species (i.e. $\cdot\text{OH}$, $\text{SO}_4^{\bullet-}$, $\text{O}_2^{\bullet-}$ and holes) were involved in the oxidation of BTA. As observed, decreasing the degradation rate in the presence of IPA was much greater than that of the other

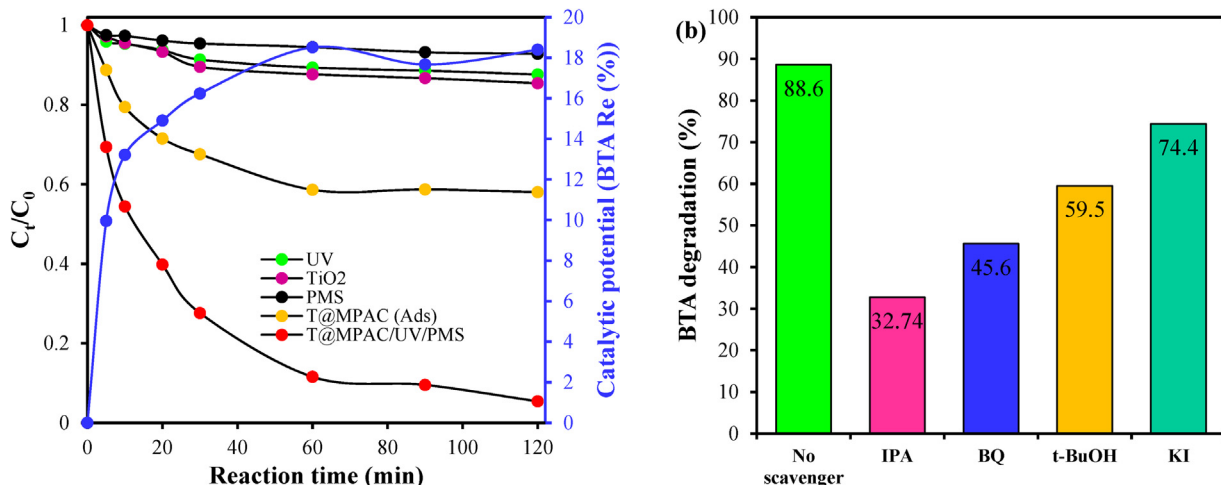


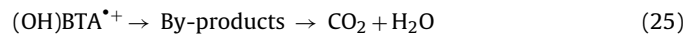
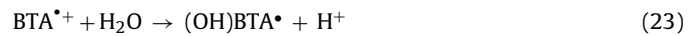
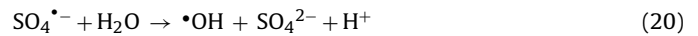
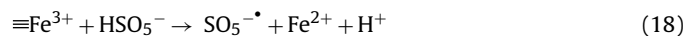
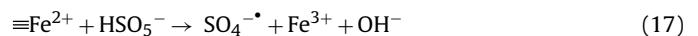
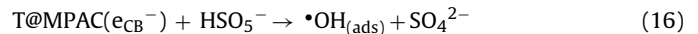
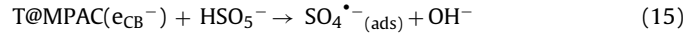
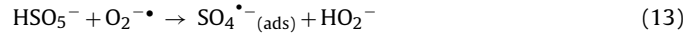
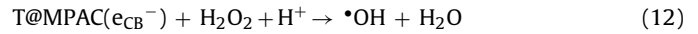
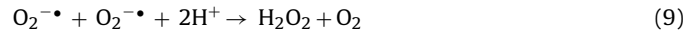
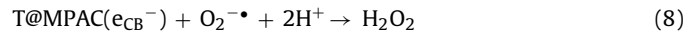
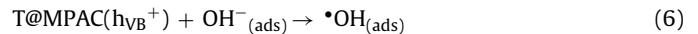
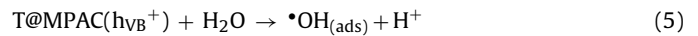
Fig. 7. (a) catalytic potential of T@MPAC in T@MPAC/PMS/UV system under optimum conditions (pH 7.0, 0.4 g/L catalyst, 4 mM PMS, 40 mg/L BTA) and (b) the effect of various reactive species scavengers on the degradation of BTA by T@MPAC/PMS/UV process (10 mM IPA, 10 mM TBA, 1 mM BQ and 10 mM KI).

scavengers. The significant inhibition effect of IPA elucidates that both •OH and SO₄^{•-} radicals participate during the degradation process of BTA. Lower decline in the degradation rate in the presence of TBA (as a specific •OH scavenger), in comparison with IPA, implies that BTA degradation was mainly affected by SO₄^{•-} radicals. As compared to TBA and KI, a strong inhibiting effect can be observed for BQ which suggests that the role of O₂^{-•} in degradation of BTA under T@MPAC/PMS/UV system is higher than that of •OH and holes. These trapping experiments elucidated that the sulfate and superoxide ion radicals play more important roles in the degradation process of BTA in T@MPAC/PMS/UV system.

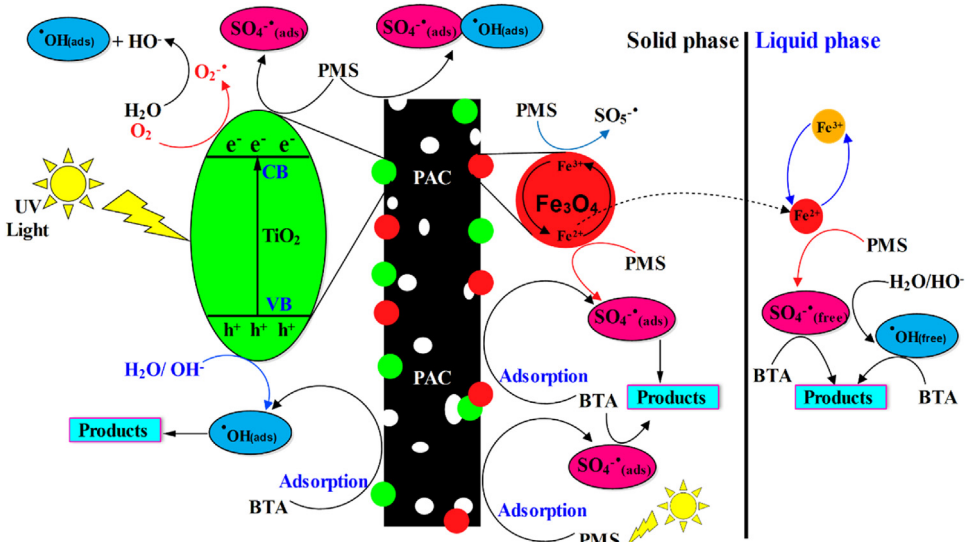
3.7. Tentative catalytic mechanism of T@MPAC/PMS/UV system

In the T@MPAC/PMS/UV system, since both TiO₂ and Fe₃O₄ nanoparticles as well as PMS present, it is expected to observe the simultaneous production of •OH and SO₄^{•-} radicals. Based on the obtained results of quenching studies, we proposed a plausible oxidation mechanism according to Scheme 1. Here, the oxidation reactions occurred both in the solution (liquid phase) and on surface of the catalyst (solid phase). Accordingly, both processes of homogeneous and heterogeneous oxidation and adsorption were involved in BTA degradation via T@MPAC/PMS/UV system. In solid phase, BTA molecules and oxidant (PMS) are adsorbed on the catalyst surface which initiate some reactions as follows [21,44]: 1) Upon UV-light of photon energy greater than band-gap energy ($\hbar\nu > E_g$), holes (h⁺) and electrons (e⁻) are generated respectively in valence and conduction bands in the TiO₂ which was loaded on the PAC surface (Eq. (4)), 2) reaction of photo-induced electrons-holes with O₂ and H₂O or OH⁻ to produce active species (HO₂[•], O₂^{-•} and •OH) according to Eqs. (5)–(7). Herein, also the generation of •OH under UV light-assisted T@MPAC photocatalysis can be occurs by O₂^{-•} species, which including production and consumption of H₂O₂ molecules, as described in Eqs. (8)–(12) [45,46]. In addition, O₂^{-•} formed can decomposed PMS molecules to generate SO₄^{•-}(ads) (Eq. (13)). Meanwhile, O₂^{-•} species would interact with H₂O molecules to generate further •OH radicals (Eq. (14)) [47], 3) the decomposition of adsorbed PMS molecules on the catalyst via the excitation of electrons conduction (Eqs. (15) and (16)), 4) the decomposition of adsorbed PMS molecules by Fe₃O₄ nanoparticles loaded on the PAC to generate SO₄^{•-}(ads) based on reactions (17) and (18) [36,48], 5) the decomposition of adsorbed PMS molecules via UV light to formation of SO₄^{•-}(ads) according to Eq. (19), and 5) oxidation of OH⁻/H₂O by SO₄^{•-} radicals to them convert into

•OH (Eqs. (20) and (21)). Finally, the oxidative degradation of the adsorbed BTA molecules was taken place on the T@MPAC catalyst by O₂^{-•}, •OH and SO₄^{•-} radicals, according to Eq. (22)–(25).



Moreover, it has been reported that the activated carbon can act as a PMS activator via the mechanism of electron transfer from surface, as described in Eqs. (26) and (27) [40,49]. Consequently, •OH and SO₄^{•-} radicals generated in the catalyst surface caused oxidation reaction of organic substrates to produce intermediates, carbon dioxide and water (Eqs. (22)–(25)). Therefore, it is expected



Scheme 1. Schematic representation of BTA degradation using T@MPAC/PMS/UV system.

that the excellent adsorption ability of PAC can improve the contact chance of BTA molecules and oxidant, led to the enhancement of degradation rate. Consequently, for T@MPAC/PMS/UV system, the catalytic activity has been substantially enhanced, due to the synergistic effect between oxidation and adsorption processes.



In liquid phase, homogeneous oxidation occurs in a similar pathway what that heterogeneous phase. There, PMS can be catalyzed through reaction between PMS and released $\text{Fe}^{II}/\text{Fe}^{III}$ from Fe_3O_4 surface, which led to the production of $\text{SO}_4^{\bullet-}(\text{free})$ (Eq. (17)). $\cdot\text{OH}(\text{free})$ radicals also formed via the interaction between $\text{SO}_4^{\bullet-}(\text{free})$ radicals and $\text{H}_2\text{O}/\text{OH}^-$ species according to Eqs. (20) and (21).

Based on this mechanism, it can be concluded that three agents; UV light-assisted photocatalysis, Fe_3O_4 MNPs and PAC were involved in the activation of PMS in the T@MPAC/PMS/UV system. Therefore, this system can represent a high degradation efficiency for organic compounds, due to the simultaneous presence of active species, significant production rate of $\cdot\text{OH}$ and $\text{SO}_4^{\bullet-}$ radicals and the excitation of the multi PMS activator.

3.8. Proposed pathway of BTA degradation

As mentioned above, BTA molecules react with reactive oxidizing species ($\cdot\text{OH}$, $\text{SO}_4^{\bullet-}$, h^+ , e^- and HO_2^{\bullet}) to produce BTA radicals and finally formation low weight by-products. As reported by other studies, we observed that at the initial times of BTA degradation process, the solution colour change to yellow-brownish and then gradually becomes completely transparent during the T@MPAC/PMS/UV process. This colour change confirms formation diaxoxime, an intermediate from the N–NH bond scission of BTA, which is consistent with observations of Ding et al., [2,50]. At the end of oxidation reactions, aniline was identified by HPLC analysis as followed the further degradation of diaxoxime, when compared with the retention time of the standard aniline (see Fig. S1). Herein, the degradation is initiated by the triazole ring opening or destroy the doubly bonded nitrogen in the triazole ring. As photochemical degradation reactions proceed aniline formed by the further reaction of diaxoxime, since it is not stable in the solution. The

decolorization of solution occurs which is probably associated with cleavage of the azo bond.

The efficient degradation of aniline by $\cdot\text{OH}$ and $\text{SO}_4^{\bullet-}$ radicals has been reported in the literature [51,52]. Huang et al. [51] detected nitroso-benzene, benzoquinone and nitrobenzene as possible intermediates of aniline degradation by $\cdot\text{OH}$ and $\text{SO}_4^{\bullet-}$ radicals during $\text{Co}_3\text{O}_4/\text{N/C}/\text{PMS}$ system. Thus, based on identified intermediates and previous studies, a reaction pathway for photocatalytic degradation of BTA are illustrated in Fig. 8.

At first, aniline was attacked by $\cdot\text{OH}$ and $\text{SO}_4^{\bullet-}$ radicals and produced benzoquinonimine (A), aniline radicals (D) and 4-amino-phenol (E). Further oxidation of benzoquinonimine by reactive oxidizing species generating maleic acid (G) through two ways: 1) benzoquinonimine hydrolyzed to benzoquinone (C) and ammonium, and then the benzene ring was opened to form maleic acid and 2) benzoquinonimine attacked by HO_2^{\bullet} and produced nitrobenzene (B), which was further degraded to maleic acid after the release of NO_3^- . Similar pathway to mineralization of benzoquinonimine have been proposed in the previous studies [51,52]. They found that the oxidation of benzoquinonimine during heterogeneous Fenton reaction and $\text{Co}_3\text{O}_4/\text{N/C}/\text{PMS}$ system yield benzoquinonimine and/or nitrobenzene, and then was degraded to maleic acid.

In other pathway, aniline radical reacts with aniline to produce 4-4'-diaminodiphenyl (F), and then was attacked by $\cdot\text{OH}$ and $\text{SO}_4^{\bullet-}$ radicals and converted to maleic acid. At the same time, 4-amino-phenol can be formed via reaction between aniline and $\cdot\text{OH}$ radicals, which was further degraded to benzoquinone. Xu et al., [2] who studied photocatalytic degradation of aniline by BiOBr, proposed that the degradation of BTA also can be directly initiated by the oxidation of hole (h^+) as well as the triazole ring opening. Afterwards, the intermediates were further degraded to 3-aminoprop-2-en-1-ol (H) by the attack of $\cdot\text{OH}$ and $\text{SO}_4^{\bullet-}$ radicals followed by deprotonation and opening of the benzene ring processes. Finally, both maleic acid and 3-aminoprop-2-en-1-ol were further mineralized to H_2O , CO_2 , and NH_4 . As conclusion, during all pathways reactive oxidizing species played main role in the BTA degrade into small molecular compounds.

3.9. Tests of reusability, stability and mineralization degree

The reusability has been reported as one of the most important factors for assessment of a catalyst since it allows for multiple

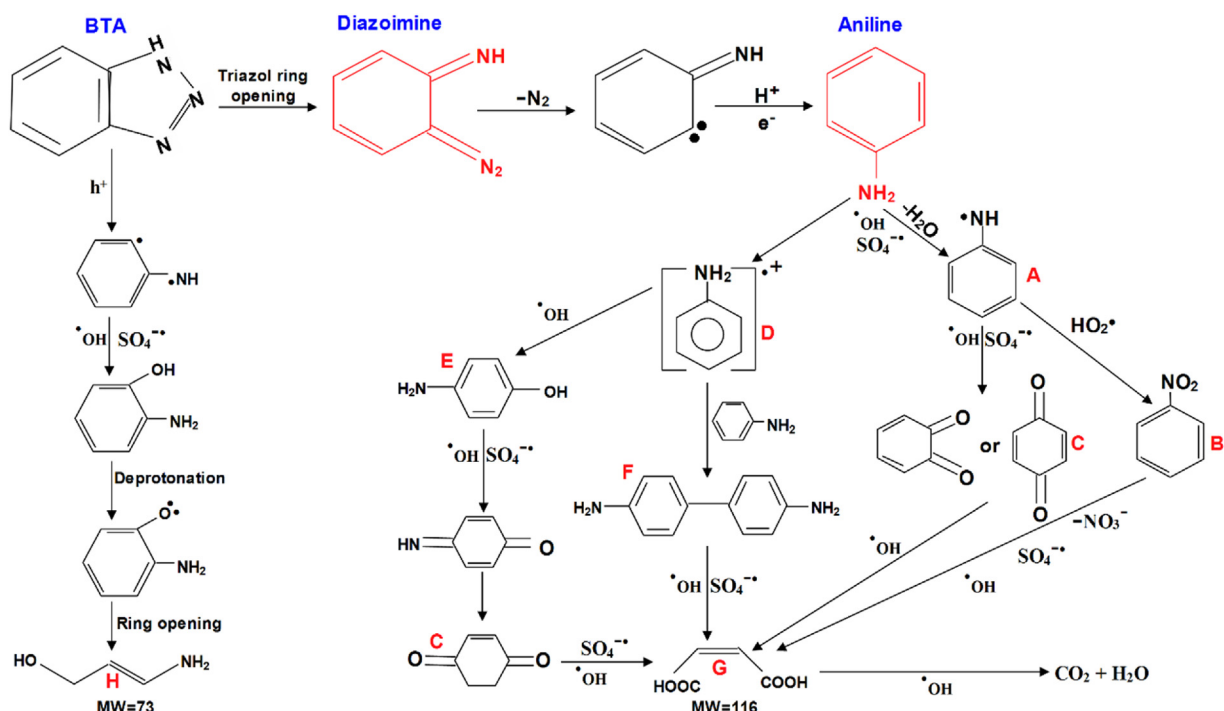


Fig. 8. Proposed reaction schemes for degradation of BTA by T@MPAC/PMS/UV system under optimum condition.

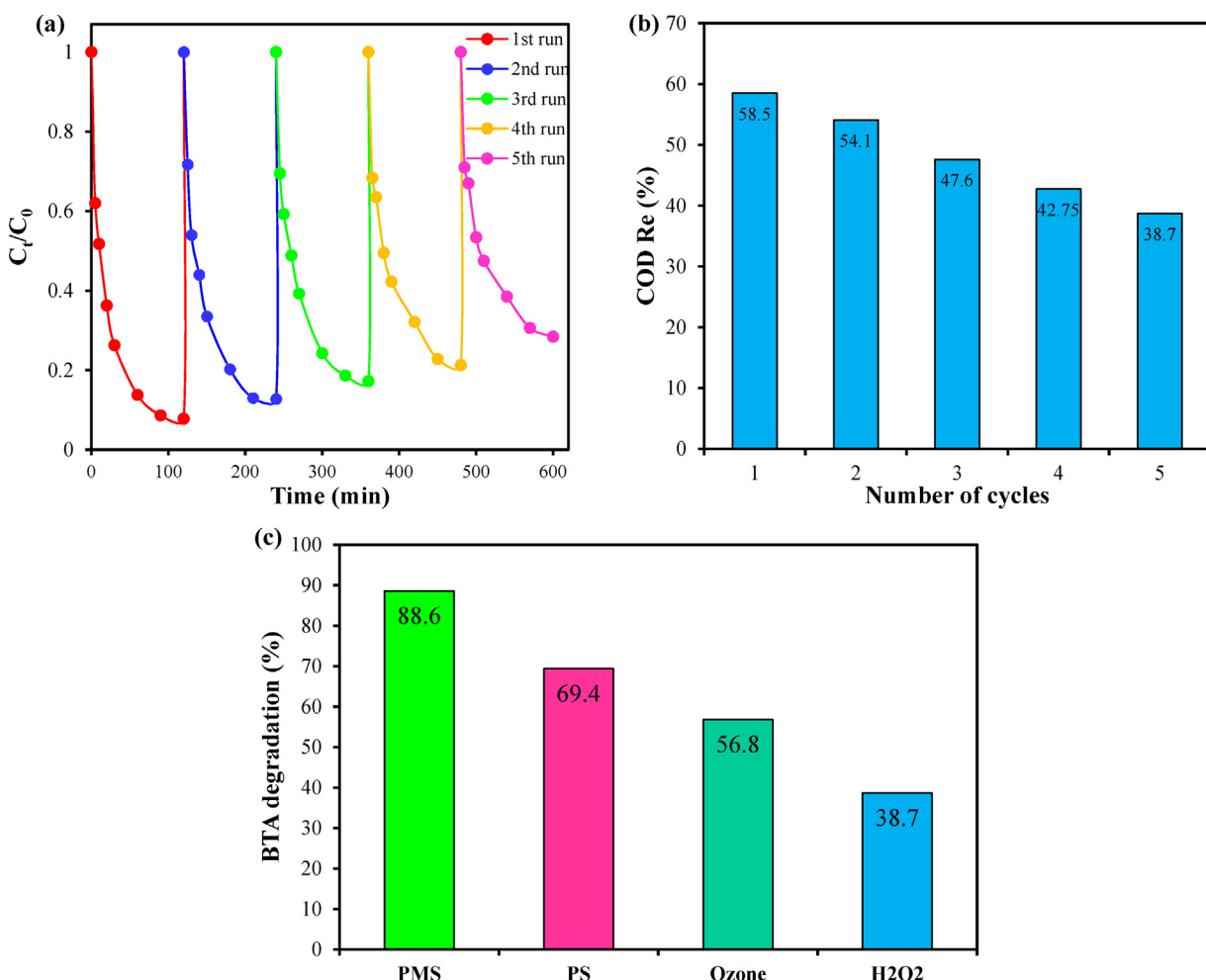


Fig. 9. (a) Reusability of as-synthesized nano-composite, (b) the mineralization degree of BTA by T@MPAC/PMS/UV process after five consecutive runs and (c) the performance of different oxidants in the degradation of BTA along with T@MPAC/UV.

applications and, therefore, will reduce costs [7]. In this work, reusability of the catalyst and its capability in mineralization of BTA in T@MPAC/PMS/UV system was evaluated for five consequent cycles under optimized conditions within 120 min reaction. Fig. 9(a) and (b) show that the degradation and mineralization efficiencies of BTA dropped insignificantly from 92.2 and 58.5% to 71.6 and 38.7%, respectively, after the fifth cycles. This means that T@MPAC has a satisfactory reusability potential and can be recycled for several times with a degradation efficiency higher 70%. Observed loss in degradation efficiency and mineralization degree might be resulted from TiO_2 and Fe_3O_4 mass loss. It also can be associated with reduce surface area of catalyst via blocking the pores on the catalyst surface by PMS and BTA molecules as well as intermediates, and the subsequently decreased the adsorption capacity of the catalyst after each cycle. Another reason for this phenomenon can be the difficulty in the complete removal of residual intermediates and reactants from the active catalytic sites in the following washing and drying procedures. Nevertheless, it expected that potential reusability of the catalyst could be reserved significantly through chemical or physical modification of the catalyst after each use. Stability experiments proved that the as-synthesized catalyst has a good stability in T@MPAC/PMS/UV system, due to the low leaching iron (<0.2 mg/L) and active species (i.e., Fe_3O_4) were strongly fixed into the mesoporous structure of the PAC.

3.10. Comparison with other oxidants

The catalytic performance of T@MPAC was compared between the different oxidants (i.e., ozone (O_3), PS and H_2O_2) in the presence of UV light under same experimental conditions. As can be seen in Fig. 9(c), high degradation of BTA was achieved in order PMS > PS > O_3 > H_2O_2 . It also displays that the sulfate-based oxidants (PMS and PS) provide better degradation efficiency, in comparison with other oxidants, suggesting that BTA is more efficiently degraded by $\text{SO}_4^{\cdot-}$ radicals, compared to $\cdot\text{OH}$ radicals. The findings of these experiments also demonstrated that T@MPAC was more successful in the activation of both PMS and PS oxidants, when it compared with the other studied oxidants. The difference in the efficiency of various oxidants can be explained by the selectivity features of sulfate radical in reaction with the organic substances.

3.11. Influence of co-existing water matrix chemicals

It is well-known that the chemical oxidation processes can be affected by the presence of anions, since they act to scavenge the free radicals and/or to generate the chlorine reactive species. The effects of chloride, nitrate, sulfate and phosphate anions were evaluated in T@MPAC/PMS/UV system on BTA removal. In this regard, the experiments were performed under obtained optimum conditions in the presence of 5 mM of anions, and the results are shown in Fig. 10(a). For all the studied anions, an inhibitory effect was observed, while none of them had favorable effect on the process performance. The performance of T@MPAC/PMS/UV system was reduced in the presence of anions. Decreasing the degradation rate of BTA in the presence of anions was as chloride > phosphate > nitrate > sulfate. The strong inhabitation effect of chloride ions is probably associated with three mechanisms; i) reaction between PMS molecules and chloride ions to generate sulfate ions (Eqs. (28)–(29)), ii) high tendency of chloride ions to react with sulfate radicals for oxidizing the chloride ions (Eqs. (30–35)) and iii) deactivating the positive holes of TiO_2 (Eq. (36)) [39,53,54]. In second way, the active chlorine species (Cl_2 , HOCl) or chlorine radicals (Cl^{\cdot} , $\text{Cl}_2^{\cdot-}$, $\text{ClO}^{\cdot-}$) can be generated as described above. It is notable that the radicals have lower reactivity than $\text{SO}_4^{\cdot-}$ radicals. When the chloride ions are present in the solution, they compete with organic compounds to react with $\text{SO}_4^{\cdot-}$, and the consequence

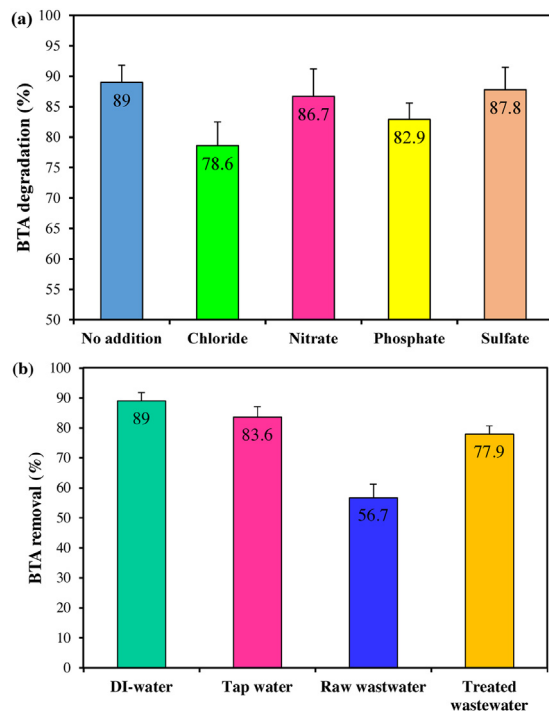
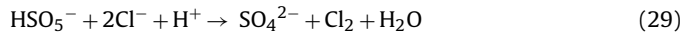


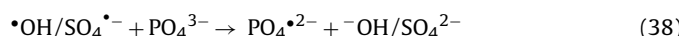
Fig. 10. Catalytic performance of T@MPAC/PMS/UV system (a) in the presence of different anions and (b) in different water matrices under optimized conditions (pH 7.0, 0.4 g/L catalyst, 4 mM PMS, 40 mg/L BTA, 5 mM anions during 70 min reaction).

is dropping the efficiency of process. Therefore, the degradation rate of BTA is decreased significantly through consumption of reactive species ($\text{SO}_4^{\cdot-}$) and decomposition of PMS molecules in a non-efficient route. Similar trends have also been reported by other researchers [39,47].



As compared to chloride ions, the other ions did not show the notable inhabitation effect on T@MPAC/PMS/UV system. For nitrate and phosphate ions, as reported in the literature, the inhabitation effect may be attributed to their act as quenching agents for scavenging of both the $\text{SO}_4^{\cdot-}$ and $\cdot\text{OH}$ radicals and formation of nitrate and phosphate radicals via electron transfer reaction (Eqs. (37) and (38)). As observed in Fig. 10(a), among the studied anions, the effect of sulfate ions was very slight on the catalytic performance of T@MPAC/PMS/UV, which comes from intrinsic of system, because it was based on $\text{SO}_4^{\cdot-}$ radicals. In T@MPAC/PMS/UV system, reducing the influence of UV light can be another reason for the loss of catalytic performance. Furthermore, the adsorption of all studied anions may occur on the catalyst surface which decreases both the adsorption capacity and catalytic surface activity of T@MPAC. Generally, during T@MPAC/PMS/UV system, anions participate in scavenging reactive species, reduce surface area and active sites

on the catalyst by blocking the pores and also decreasing catalyst potential in the activation of PMS.



3.12. Treatment of real water and wastewater

To evaluate the efficiency of T@MPAC/PMS/UV system in practical applications, its performance was examined in the real samples treatment of water and wastewater. In this regard, tap water, raw and treated (secondary effluent) municipal wastewater were applied as real samples and their characteristics are given in Table S-3. BTA concentration was set at 40 mg/L for all the samples and the experiments were conducted under the optimized conditions. According to Fig. 10(b), BTA degradation rate for all studied real samples was lower than that of DI-water. The removal efficiencies of 89, 83.6, 56.7 and 77.9% were obtained respectively in DI-water, tap water, raw and treated wastewater samples. In case of tap water, a high total dissolved suspended (TDS), which has inhibiting effect, reduced the catalytic performance of T@MPAC/PMS/UV system via quenching the free radicals. A low efficiency for raw wastewater sample is presumably associated with the existence of solids and interfering ions and/or the other organic pollutants. Therein, both compete between organic substances and BTA molecules for reaction with reactive species as well as the presence of high concentrations of quenching agents, lead to decreasing BTA removal. The relatively small reduction of degradation rate in treated wastewater sample also may be attributed to the organic compounds competing in the wastewater. As a conclusion, T@MPAC/PMS/UV system shows an excellent catalytic performance in the oxidative degradation of organic pollutants in real samples. Therefore, it can be employed as an efficient and promising technique for effective treatment of water and wastewater.

4. Conclusion

In this paper, PMS was used as an effective agent for increasing the efficiency of the heterogeneous photocatalyst system (T@MPAC/UV) in the degradation of BTA. A high degradation efficiency (>92.2%) was achieved during BTA degradation by T@MPAC/PMS/UV system. This high performance was related to the simultaneous participation of the adsorption, UV-Fenton and photocatalyst processes. Results revealed that the C and E had respectively the highest negative and positive effects on the removal efficiency of BTA. Among the reactive species (i.e. $\cdot\text{OH}$, $\text{SO}_4^{\bullet-}$, $\text{O}_2^{\bullet-}$ and holes) included in T@MPAC/PMS/UV system, $\text{SO}_4^{\bullet-}$ radicals had dominant role in controlling the oxidation reaction. T@MPAC shows also a better performance in the activation of PMS, compared to the other studied oxidants. After 5 times of reuse cycles, the degradation efficiency of BTA dropped from 92.2 to 71.6%, which confirmed the excellent potential reusability of as-synthesized nanocomposite. Ultimately, the toxicity for the degradation intermediates and also application in the full-scale could be further studied in the future to accomplish economic design.

Acknowledgment

The funding of the present research has been provided by the Environmental Technologies Research Center, Ahvaz Jundishapur University of Medical Sciences (Grant No. ETRC-9607).

Appendix A. Supplementary data

Supplementary data associated with this article can be found, in the online version, at <http://dx.doi.org/10.1016/j.apcatb.2017.07.035>.

References

- [1] M. Ahmadi, B. Kakavandi, S. Jorfi, M. Azizi, *J. Photochem. Photobiol. A: Chem.* 336 (2017) 42–53.
- [2] J. Xu, L. Li, C. Guo, Y. Zhang, S. Wang, *Chem. Eng. J.* 221 (2013) 230–237.
- [3] B. Roshani, I. McMaster, E. Rezaei, J. Soltan, *Sep. Purif. Technol.* 135 (2014) 158–164.
- [4] Z. Zhang, N. Ren, Y.-F. Li, T. Kunisue, D. Gao, K. Kannan, *Environ. Sci. Technol.* 45 (2011) 3909–3916.
- [5] H.-L. Cheng, Z.-S. Huang, L. Wang, H. Meier, D. Cao, *Dyes Pigm.* 137 (2017) 143–151.
- [6] B. Kakavandi, A.A. Babaei, *RSC Adv.* 6 (2016) 84999–85011.
- [7] A. Jonidi Jafari, B. Kakavandi, N. Jaafarzadeh, R. Rezaei Kalantary, M. Ahmadi, A. Akbar Babaei, *J. Ind. Eng. Chem.* 45 (2017) 323–333.
- [8] S. Wang, S. Zhou, *Appl. Surf. Sci.* 256 (2010) 6191–6198.
- [9] Q. Lv, G. Li, H. Sun, L. Kong, H. Lu, X. Gao, *Microporous Mesoporous Mater.* 186 (2014) 7–13.
- [10] S. Liu, M. Lim, R. Amal, *Chem. Eng. Sci.* 105 (2014) 46–52.
- [11] H.U. Lee, G. Lee, J.C. Park, Y.-C. Lee, S.M. Lee, B. Son, S.Y. Park, C. Kim, S. Lee, S.C. Lee, *Chem. Eng. J.* 240 (2014) 91–98.
- [12] B. Kakavandi, M. Jahangiri-rad, M. Rafiee, A.R. Esfahani, A.A. Babaei, *Microporous Mesoporous Mater.* 231 (2016) 192–206.
- [13] A.J. Jafari, B. Kakavandi, R.R. Kalantary, H. Gharibi, A. Asadi, A. Azari, A.A. Babaei, A. Takdastan, *Korean J. Chem. Eng.* 33 (2016) 2878–2890.
- [14] B. Kakavandi, A. Jonidi Jafari, R. Rezaei Kalantary, S. Nasseri, A. Esrafil, A. Gholizadeh, A. Azari, *J. Chem. Technol. Biotechnol.* 91 (2016) 3000–3010.
- [15] Y. Ao, J. Xu, X. Shen, D. Fu, C. Yuan, *J. Hazard. Mater.* 160 (2008) 295–300.
- [16] Y. Ao, J. Xu, D. Fu, X. Shen, C. Yuan, *Sep. Purif. Technol.* 61 (2008) 436–441.
- [17] M. Ahmadi, H. Ramezani Motlagh, N. Jaafarzadeh, A. Mostoufi, R. Saeedi, G. Barzegar, S. Jorfi, *J. Environ. Manage.* 186 (Part 1) (2017) 55–63.
- [18] A.A. Babaei, A. Azari, R.R. Kalantary, B. Kakavandi, *Water Sci. Technol.* 72 (2015) 1988–1999.
- [19] A. Banisharif, A.A. Khodadadi, Y. Mortazavi, A.A. Firooz, J. Beheshtian, S. Agah, S. Menbari, *Appl. Catal. B: Environ.* 165 (2015) 209–221.
- [20] S. Yang, T. Xiao, J. Zhang, Y. Chen, L. Li, *Sep. Purif. Technol.* 143 (2015) 19–26.
- [21] Y. Ren, L. Lin, J. Ma, J. Yang, J. Feng, Z. Fan, *Appl. Catal. B: Environ.* 165 (2015) 572–578.
- [22] A.A. Aziz, K.S. Yong, S. Ibrahim, S. Pichiah, *J. Hazard. Mater.* 199 (2012) 143–150.
- [23] D. Du, W. Shi, L. Wang, J. Zhang, *Appl. Catal. B: Environ.* 200 (2017) 484–492.
- [24] M.S. Nahar, K. Hasegawa, S. Kagaya, S. Kuroda, *Sci. Technol. Adv. Mater.* 8 (2007) 286–291.
- [25] J. Huang, X. Li, M. Ma, D. Li, *Chem. Eng. J.* 314 (2017) 182–191.
- [26] M. Ahmadi, B. Kakavandi, S. Jorfi, M. Azizi, *J. Photochem. Photobiol. A: Chem.* 336 (2017) 42–53.
- [27] American Society for Testing and Material (ASTM), 2012.
- [28] M. Ahmadi, M. Foladivanda, N. Jaafarzadeh, Z. Ramezani, B. Ramavandi, S. Jorfi, B. Kakavandi, *J. Water Supply: Res. Technol.-Aqua* 66 (2017) 116–130.
- [29] E.K. Pasandideh, B. Kakavandi, S. Nasseri, A.H. Mahvi, R. Nabizadeh, A. Esrafil, R.R. Kalantary, *J. Environ. Health Sci. Eng.* 14 (2016) 1–13.
- [30] K.-Y.A. Lin, Z.-Y. Zhang, *Chem. Eng. J.* 313 (2017) 1320–1327.
- [31] S. Khan, X. He, J.A. Khan, H.M. Khan, D.L. Boccelli, D.D. Dionysiou, *Chem. Eng. J.* 318 (2017) 135–142.
- [32] D. Kanakaraju, J. Kockler, C.A. Motti, B.D. Glass, M. Oelgemöller, *Appl. Catal. B: Environ.* 166 (2015) 45–55.
- [33] H. Meng, W. Hou, X. Xu, J. Xu, X. Zhang, *Particuology* 14 (2014) 38–43.
- [34] J. Lu, C. Deng, X. Zhang, P. Yang, *ACS Appl. Mater. Interfaces* 5 (2013) 7330–7334.
- [35] L. Duan, B. Sun, M. Wei, S. Luo, F. Pan, A. Xu, X. Li, *J. Hazard. Mater.* 285 (2015) 356–365.
- [36] C. Cai, H. Zhang, X. Zhong, L. Hou, *J. Hazard. Mater.* 283 (2015) 70–79.
- [37] M. Stoyanova, I. Slavova, V. Ivanova, *Appl. Catal. A: Gen.* 476 (2014) 121–132.
- [38] S. Luo, L. Duan, B. Sun, M. Wei, X. Li, A. Xu, *Appl. Catal. B: Environ.* 164 (2015) 92–99.
- [39] J. Sharma, I. Mishra, D.D. Dionysiou, V. Kumar, *Chem. Eng. J.* 276 (2015) 193–204.
- [40] W.-D. Oh, S.-K. Lua, Z. Dong, T.-T. Lim, *J. Hazard. Mater.* 284 (2015) 1–9.
- [41] X. Wang, J. Song, J. Huang, J. Zhang, X. Wang, R. Ma, J. Wang, J. Zhao, *Appl. Surf. Sci.* 390 (2016) 190–201.
- [42] W. Li, Y. Tian, C. Zhao, Q. Zhang, W. Geng, *Chem. Eng. J.* 303 (2016) 282–291.
- [43] M. Ahmadi, B. Kakavandi, N. Jaafarzadeh, A. Akbar Babaei, M. Ahmadi B, B. Kakavandi N. Jaafarzadeh A. Akbar Babaei Sep. Purif. Technol., *Sep. Purif. Technol.* 177 (2017) 293–303.
- [44] Y. Liu, H. Guo, Y. Zhang, W. Tang, X. Cheng, H. Liu, *Chem. Phys. Lett.* 653 (2016) 101–107.

[45] S. Khan, C. Han, H.M. Khan, D.L. Boccelli, D.D. Dionysiou, S. Khan C. Han H.M. Khan D.L. Boccelli D.D. Dionysiou *J. Mol. Catal. A: Chem.*, *J. Mol. Catal. A: Chem.* 428 (2017) 9–16.

[46] X. Qian, M. Ren, Y. Zhu, D. Yue, Y. Han, J. Jia, Y. Zhao, X. Qian M. Ren Y. Zhu D. Yue Y. Han J. Jia Y. Zhao *Environ. Sci. Technol., Environ. Sci. Technol.* 51 (2017) 3993–4000.

[47] Y. Liu, H. Guo, Y. Zhang, W. Tang, X. Cheng, H. Liu, *Chem. Phys. Lett.* 653 (2016) 101–107.

[48] Y. Xu, J. Ai, H. Zhang, *J. Hazard. Mater.* (2016).

[49] E. Saputra, S. Muhammad, H. Sun, S. Wang, *RSC Adv.* 3 (2013) 21905–21910.

[50] Y. Ding, C. Yang, L. Zhu, J. Zhang, *J. Hazard. Mater.* 175 (2010) 96–103.

[51] Q. Huang, J. Zhang, Z. He, P. Shi, X. Qin, W. Yao, *Chem. Eng. J.* 313 (2017) 1088–1098.

[52] Y. Liu, G. Zhang, S. Fang, S. Chong, J. Zhu, *J. Environ. Manage.* 182 (2016) 367–373.

[53] F. Qi, W. Chu, B. Xu, *Chem. Eng. J.* 235 (2014) 10–18.

[54] Y. Ji, Y. Fan, K. Liu, D. Kong, J. Lu, *Water Res.* 87 (2015) 1–9.